Chapter 14

Probing the Interface of Charged Surfactants in Ionic Liquids by XPS

Lang G. Chen and Harry Bermudez*

Department of Polymer Science and Engineering, University of Massachusetts, 120 Governors Drive, Amherst, Massachusetts 01003
***E-mail: bermudez@polysci.umass.edu**

Room-temperature ionic liquids (ILs) are playing increasingly vital roles in many processes of both fundamental and applied natures such as separations and catalysis. It is therefore critical to obtain a better understanding of their interfacial properties such as surface charge and composition. Here we examine the influence of positively-charged surfactants on IL interfaces by X-ray photoelectron spectroscopy (XPS). The roles of surfactant alkyl chain length, concentration, and information depth on interfacial properties are investigated. XPS provides detailed compositional information that is used to calculate properties such as surface activity, composition, and charge. Depending on the chain length and concentration, the surfactants can alter the IL interface to varying extents, highlighting a simple route to manipulate interfacial properties. Our results are a further demonstration of the ability of XPS to give insights into the surface activity and aggregation behavior in multi-component ionic liquid systems.

In Ionic Liquids: Science and Applications; Visser, A., et al.;
ACS Symposium Series; American Chemical Society: Washington, DC, 2012.

Introduction

Room-temperature ionic liquids (ILs), organic salts with a melting point below 100 °C, continue to receive intense attention because of their unusual and diverse properties. The nature of the IL interface is of central importance in applications such as catalysis, chromatography, and fuel cells (*1–5*). The self-assembly of amphiphilic molecules such as surfactants in ILs is also of fundamental interest to the field of colloid and interface science (*6–10*).

Because of the negligible vapor pressure of ILs, ultrahigh vacuum (UHV) techniques can be used to interrogate IL surface and bulk properties (*11–18*). The application of UHV based techniques including X-ray photoelectron spectroscopy (XPS), secondary ion mass spectrometry (SIMS) (*12*), metastable impact electron spectroscopy (MIES) (*19*), direct recoil spectroscopy (*20*), and low-energy ion scattering (LEIS) (*21*), provides insight into both chemistry and surface properties at molecular length scales. Other surface-sensitive methods without UHV conditions include sum frequency generation (SFG) (*22*, *23*), X-ray reflectivity (*23*, *24*), and surface tension measurements (*25–27*). Among all of these techniques, XPS is arguably the most common and prominent UHV-based tool to provide unique information on chemical composition, chemical state identification and even composition depth profiles of the near-surface region. A comprehensive review article was recently published by Lovelock et al. (*28*) on photoelectron spectroscopy applied to IL interfaces. Since the first work on XPS of ILs at the IL-air interface reported by Smith et al. (*11*) and Caporali et al. (*21*) in 2005, there have been many XPS studies on the influence of anions (*15*) and substituents (*16*) on the surface composition of neat ILs. Other XPS studies have sought to reveal the orientation of ions at the interface (*14*), to monitor organic reactions in ILs (*29*) and to characterize novel IL materials such as amino acid based ionic liquids (*30*). XPS has also been used to investigate surface enhancement and solubility of salts dissolved in ILs (*18*, *31*). However, few studies have examined more complex systems such as surfactant-IL mixtures. Through the introduction of (charged) surfactants, the interfacial properties such as surface tension, composition, and charge can be tuned and controlled. More importantly, these properties can be quantitatively characterized by XPS.

This chapter intends to highlight opportunities in colloid and interface science made possible by the unique properties of ionic liquids and the strengths of XPS. While the ability of ILs to solubilize a wide variety of compounds is of clear interest and continues to be studied (*32–38*), mixtures that include ILs have complex phase behavior that is relevant to many potential applications. For example, the formation of microemulsions or other dispersed phases can be facilitated and controlled through the use of amphiphilic molecules (*39*). At a more basic level, ionic liquids provide a window to re-examine our understanding of solubility and aggregation phenomena, which is most often based on our experiences with water, a unique solvent itself. To begin addressing some of these questions, we have used a model hydrophilic ionic liquid, 1-ethyl-3-methylimidazolium ethyl sulfate, more commonly referred to as [EMIM][$EtSO_4$] (see Figure 1). This imidazolium ionic liquid has been

widely studied (*12*, *13*, *40–43*) and is miscible with water in all proportions. Alkyltrimethylammonium bromides with different alkyl chain lengths were chosen as model ionic surfactants.

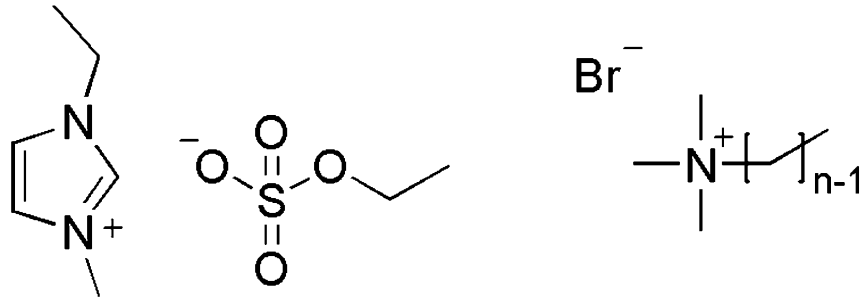

Figure 1. Structures of ionic liquid and surfactants in this study.

Experimental

Materials

[EMIM][$EtSO_4$] was obtained from Sigma (>95%). The ionic liquid was dried by heating at 70°C under vacuum for 2 days. The purity of the neat ionic liquid, and selected surfactants, were assessed by ^{1}H-NMR and did not reveal any impurities. These findings were confirmed by subsequent XPS control experiments (*41*).

Dodecyltrimethylammonium bromide (C_{12}TAB) (99%) was purchased from Fisher. Hexyltrimethylammonium bromide (C_6TAB) (>98%), octyltrimethylammonium bromide (C_8TAB) (>98%), decyltrimethylammonium bromide (C_{10}TAB) (>98%), and tetradecyltrimethylammonium bromide (C_{14}TAB) (>99%) were purchased from Sigma. All surfactants were used as received.

Tensiometry

Surface tension was measured by the Wilhelmy method using a Micro Trough XS (Kibron, Finland). For room temperature isotherms, the samples of alkyltrimethylammonium bromides were prepared and investigated as described in a previous report (*41*). Briefly, after all surfactants were dissolved in reverse-osmosis water, between 5 and 40μL of aqueous solutions were applied onto the ionic liquid subphase with volume of 300-500μL. We note that although water is introduced in the application of surfactant, it is always less than 12% by volume and does not significantly alter the bare surface tension ($\Delta\gamma < 3\%$), which was also found by Marsh et al (*44*). Surface tensions were measured after an equilibration time of 15 min.

X-ray Photoelectron Spectroscopy

Samples for XPS were prepared and investigated the same way as in a previous report (*41*). 5μL of aqueous surfactant solutions were applied onto the surface of 5μL of IL droplets using (oxygen-plasma-cleaned) silicon wafers as substrates. Samples were dried in a flowing nitrogen environment for 3 days at room temperature prior to conducting XPS measurement. XPS data were recorded using a Physical Electronics Quantum 2000 Microprobe instrument with monochromatic Al X-rays at 50 W, and a 200 μm spot area. Atomic compositions were obtained by using known sensitivity factors for the instrument and setup. To determine molecular compositions, atomic mass balances were performed using the chemical formulas of each species (for details see Chen et al. (*41*)). Importantly, the purity of the neat IL and the negligible influence of water and nitrogen introduced during preparation were confirmed by several different XPS control experiments (*41*).

Results and Discussion

The phase behavior of ionic surfactants is complex and depends on the solvent, concentration, and temperature. For example, micellization only occurs above a critical concentration and critical temperature, referred to as the critical micelle concentration (cmc) and Krafft temperature (T_k), respectively. We have recently shown that Krafft temperatures for ionic surfactants in ILs are generally much higher than room temperature (*43*). As a consequence, surface tension measurements at room temperature do not entirely reflect the phase behavior of surfactants, in particular at high concentrations (Figure 2). Because our XPS measurements were conducted at room temperature, these results are not complicated by the potential appearance of micelles. Of course, at sufficiently high surfactant concentrations, a separate solid phase will appear in equilibrium with the liquid phase. At low surfactant concentrations, interfacial properties will not be substantially altered – at least until a surface monolayer has been established. Indeed, as was first noted by Rayleigh (*45*) the first break in plots of surface tension vs. concentration (i.e., isotherms) marks the onset of this condensed phase (Figure 2). Here we denote this transition concentration as C_a, and it furthermore provides a useful reference point. For example, using a relative concentration $C^* \approx 10C_a$ allows us to compare surfactants of different chain lengths in a more meaningful way than on an absolute basis (e.g., Figure 3).

Table 1 lists both the transition concentrations (C_a) and critical micelle concentrations (cmc) of C_nTAB in [EMIM][$EtSO_4$] and in water. As noted earlier, the cmc can only be attained above the Krafft temperature. Although the C_a is a function of temperature, the values reported here are at room temperature to facilitate interpretation of the XPS measurements. Our own cmc determinations in water are consistent with literature values (*46*, *47*) and these cmc are generally lower than those in ionic liquids, indicating the well-known behavior of greater solubility in ionic liquids.

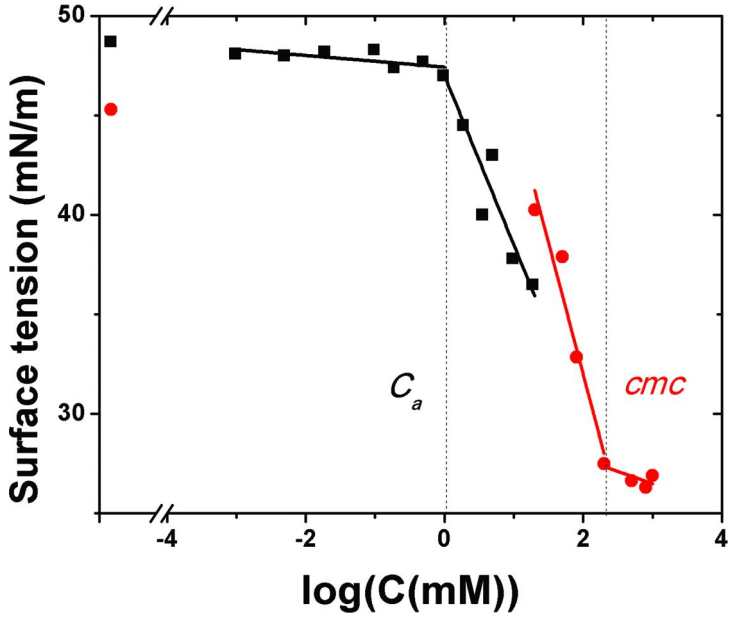

Figure 2. Isotherms of $C_{14}TAB$ in [EMIM][$EtSO_4$] at different temperatures: 20°C (squares) and 90°C (circles). The surface tensions of neat IL at different temperatures are shown as the first points before the break. The Krafft temperature for this system is T_k = 75°C (43).

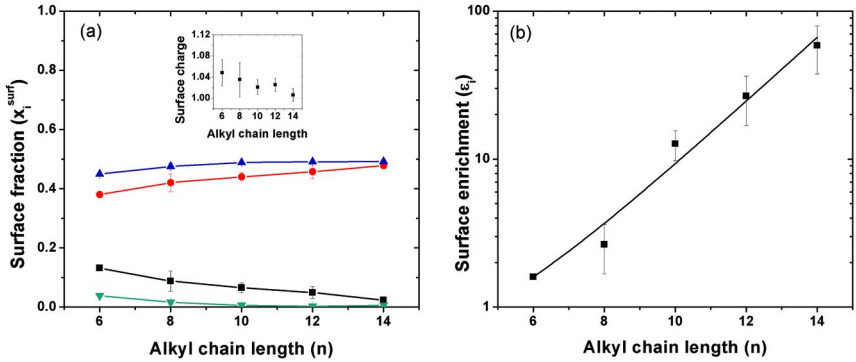

Figure 3. (a) Surface fractions, x_i^{surf}, (C_nTA^+ (squares), $[EMIM]^+$ (circles), $[EtSO_4]^-$ (top triangles), and Br^- (bottom triangles) and overall surface charge ratios (inset) and (b) surface enrichment of C_nTAB on [EMIM][$EtSO_4$]. Overall surface charge is defined as the ratio of total surface cations to total surface anions. Surface enrichment is defined as the ratio $\varepsilon_i = x_i^{surf} / x_i^{bulk}$, where x_i^{surf} are taken over the XPS information depth d ≈ 3.2 nm.

In Ionic Liquids: Science and Applications; Visser, A., et al.;
ACS Symposium Series; American Chemical Society: Washington, DC, 2012.

Table 1. Alkyltrimethylammonium Bromide Transition Concentrations and Critical Micelle Concentrations, in mM, Determined by Tensiometry

Chain length	*[EMIM][EtSO$_4$]*		*water*		
	C_a *(90°C)*	cmc_{exp} *(90°C)*	C_a *(20°C)*	cmc_{exp} *(20°C)*	cmc_{ref} *(25°C)*
6	70	5100	/	/	990 (*46*)
8	33	3300	43	380	261 (*46*)
10	6.0	2000	4.3	69	64.6 (*47*)
12	1.4	510	2.2	14.8	14.2 (*47*)
14	0.6	190	0.03	3.1	3.6 (*47*)

Chain Length Effect

Analysis of XPS data typically involves decoupling signal peaks into contributions from particular elemental types based on their respective binding energies (*12–15*). However, this process is complicated in our systems due to the increased number of species: two ions from the IL and two ions from the surfactant. We therefore analyzed the elemental composition data by means of atomic mass balances (*48*, *49*), which only rely on the presence of one or more unique atomic species (e.g., nitrogen or sulfur). In essence, this approach simply accounts for the relative amounts of a given element within each molecular species (*41*). Once the compositions of all molecular species are determined, numerous additional quantities may be calculated. The mole fractions of each species x_i^{surf} gives an effective surface concentration averaged over the information depth $d \approx$ 3.2 nm (based on an emission angle of 45°) which is greater than the molecular lengths of the ions and surfactants (*50*, *51*). Figure 3(a) shows the surface fractions of each species in the C_nTAB / [EMIM][$EtSO_4$] mixtures. It can be seen that the IL components always remain the major surface species, which is likely due to the relatively low overall concentration of surfactants. As mentioned earlier, the *bulk* concentration for each mixture is fixed at $C^* \approx 10C_a$. In spite of this normalized concentration, the shorter chain length surfactants are more abundant near the surface than their longer counterparts are.

To more carefully consider the effect of surfactant chain length, we define "surface enrichment" as the ratio of surface fraction to bulk fraction, $\varepsilon_i = x_i^{surf}/x_i^{bulk}$, which provides a measure of the relative tendency of a species to segregate to the interface (i.e., for an ideal mixture $\varepsilon_i = 1$). We find that all C_nTA^+ surfactants exhibit surface enrichments $\varepsilon \gg 1$, confirming their surface activity at the IL interface (Figure 3(b)). Therefore, XPS can be used as a direct measure of surface activity even in mixtures, which may prove advantageous in situations where tensiometry is either not possible or inconvenient. Furthermore, ε increases exponentially with chain length, which we presume to be due to IL solvatophobicity, analogous to the hydrophobic effect in water (*50*). A key result

In Ionic Liquids: Science and Applications; Visser, A., et al.;
ACS Symposium Series; American Chemical Society: Washington, DC, 2012.

of Figure 3 is that while the surface fraction of longer surfactants (e.g., $C_{14}TA^+$) is not particularly large, they are partitioning to the interface much more efficiently than shorter surfactants. We also note that the surfactant Br^- counterions are undetectable (below 0.1 atomic %) at the interface for longer surfactants, suggestive of nearly complete dissociation. This situation is in stark contrast to C_nTAB behavior in water, where a significant fraction of Br^- counterions remains bound to the surfactant (or micelle) (*52*). Our observation of Br^- dissociation is consistent with earlier studies reporting the dissociation of halides in ILs (e.g., Cl^- from $[Pt(NH_3)_4]Cl_2$ in [EMIM][$EtSO_4$]) (*18*, *20*). The surface enrichment of C_nTA^+ and simultaneous dissociation of Br^- indicate a complex interplay among the various charged species. Previous work from our group (*41*) with anionic surfactants shows similar surface fraction and enrichment effects which suggest that this behavior does not depend on the specific chemical identity of the ionic surfactant. We are currently exploring the importance of counterions more carefully through the examination of zwitterionic and catanionic surfactants.

Another quantity that is directly determined from the XPS compositional data is the overall surface charge, defined here as the ratio of total cations to total anions. We again emphasize that this property is defined over the information depth $d \approx 3$ nm. This ratio is expected to be unity due to the condition of electroneutrality and we find that the surface charge ratio is 1.01±0.03 for neat [EMIM][$EtSO_4$] (N = 27), which implies a slight net positive charge of the IL. However, considering the relative error of the XPS experiments, the overall surface charge is indeed close to electroneutrality. As shown in the inset of Figure 3(a), the surface charge ratio shows significant overlap with that of the neat [EMIM][$EtSO_4$] for all surfactant chain lengths. If we recall that $C^* \approx 10C_a$, it seems plausible to interpret this effect to be a result of both IL ions being the majority species at the interface.

Concentration Effects

To further examine the influence of surfactants on IL interfacial properties, we varied the surfactant concentration for two specific chain lengths: n=8 and n=14. With increasing C_8TAB surfactant concentration, the fractions of $[EMIM]^+$ and $[EtSO_4]^-$ both decrease, while the fractions of C_8TA^+ and its counterion Br^- both increase (Figure 4(a)). This trend reflects a dynamic ion exchange process near the interface, where one cation type progressively exchanges with the other. A similar trend is observed for the anions. This exchange of ions does not continue indefinitely, since the C_8TA^+ and Br^- fractions appear to reach a plateau at high concentrations. Such behavior suggests that even below the Krafft temperature, the interface achieves complete saturation with C_8TA^+ at a concentration near the cmc. This scenario would be consistent with surface tension-concentration isotherms carried out *above* the Krafft temperature, where the cmc can be clearly identified. However, since the XPS experiments were conducted at room temperature, a second solid phase must appear at high surfactant concentrations, and certainly before the cmc. We are led to conclude that the solid phase of C_8TA^+ is minimally surface-active in [EMIM][$EtSO_4$].

In Ionic Liquids: Science and Applications; Visser, A., et al.;
ACS Symposium Series; American Chemical Society: Washington, DC, 2012.

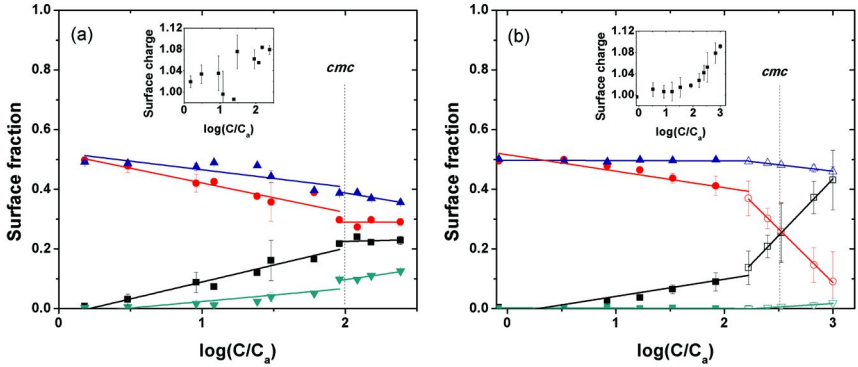

Figure 4. Surface fractions (C_nTA^+ (squares), $[EMIM]^+$ (circles), $[EtSO_4]^-$ (top triangles), and Br^- (bottom triangles) and surface charge ratios (inset) of (a) C_8TAB and (b) $C_{14}TAB$ in $[EMIM][EtSO_4]$. The open symbols represent samples that exhibit a semi-solid surface film.

For the longer $C_{14}TAB$ surfactant, the fraction of $C_{14}TA^+$ increases with concentration and appears to cross a transition point, beyond which it increases more steeply (Figure 4(b)). In this second regime the ion exchange of the two cations ($C_{14}TA^+$ and $[EMIM]^+$) reaches completeness, that is, their fractions become equal. Curiously, this point of equality coincides almost exactly with the cmc, even though once again the system is below the Krafft temperature. The fractions of both anions (Br^- and $[EtSO_4]^-$) remain more or less constant irrespective of the surfactant concentration. Therefore, in contrast to the situation with C_8TAB, for $C_{14}TAB$ there are fewer species are participating in the ion exchange process. The concentration-dependent differences in behavior for C_8TAB and $C_{14}TAB$ might due to several reasons, possibly including that $C_{14}TA^+$ is substantially more surface active than C_8TA^+ (Figure 3(b)). Furthermore, at high $C_{14}TAB$ concentrations we observed the formation of semi-solid surface layer, which is suggestive of a multilayer film (the open symbols in Figure 4(b) are used in this case). This type of film would be possible if $C_{14}TA^+$ retains significant surface activity below its Krafft temperature, but further investigation is needed to clarify the nature of this interface.

Even at high $C_{14}TAB$ concentrations, the Br^- counterion is minimally present while the $[EtSO_4]^-$ anion is about half of the total surface fraction. A possible reason for this behavior is that the intermolecular attraction between $C_{14}TA^+$ and $[EtSO_4]^-$ is stronger than that between $C_{14}TA^+$ and Br^-. The former interaction would clearly contain a van der Waals contribution whereas the latter would be primarily of an electrostatic nature. Results from our own previous work and that of others have indicated the possibility of highly effective charge screening within ILs (*53–55*), which would support an interaction between C_nTA^+ and $[EtSO_4]^-$ that increases with chain length due to van der Waals attraction. While the low polarizability of halides could also explain the low Br^- surface fraction (*18*), this effect would be independent of the surfactant.

At low surfactant concentrations, the surface charge remains close to that of the neat IL (insets in Figure 4). However, for both surfactants there is an increasing trend with concentration, ultimately crossing into the positive charge regime. In the case of C_{14}TAB, this elevated positive surface charge may reflect the presumed formation of a multilayer at the interface. We note that other effects, such as the strength of ion-pairing between the IL ions (*53*, *54*, *56*), or local heterogeneities within the IL (*57–60*), may be important factors in determining whether surface charge can be altered by surfactants. Indeed, angle-resolved studies have revealed surface layering of ions, which leads to a composition profile that oscillates with depth (*24*, *61*).

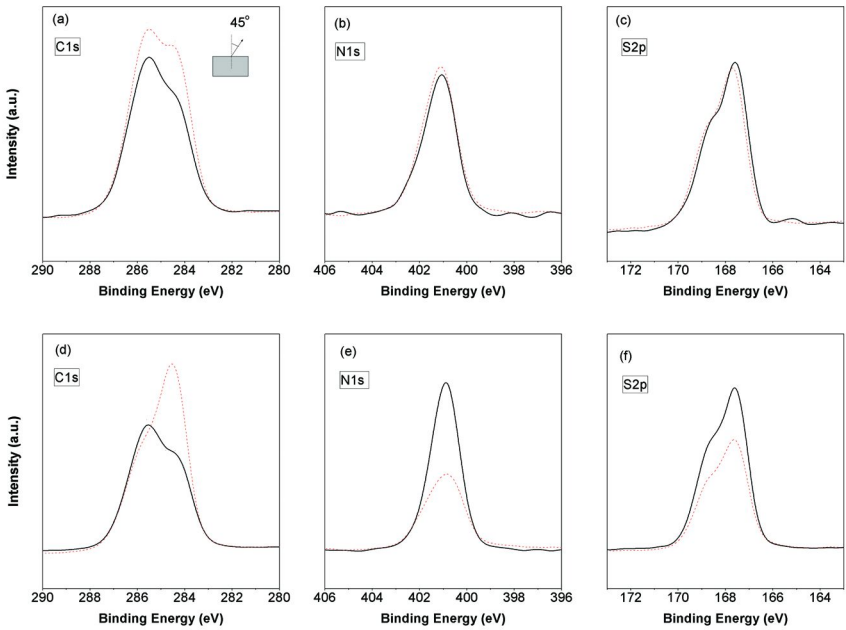

Figure 5. Detailed X-ray photoelectron spectra of (a, b, c) C_8TAB and (d, e, f) C_{14}TAB in [EMIM][$EtSO_4$] at two different surfactant concentrations. The solid lines represent $C \approx 30C_a$ < cmc, while the dashed lines represent C > cmc. The spectra were taken with an emission angle of 45° (information depth d ≈ 3.2 nm).

In Figure 5, selected X-ray photoelectron spectra of C1s, N1s, and S2p are presented to illustrate the effects of chain length and concentration. For both C_8TAB and C_{14}TAB surfactants, the C1s peak intensity increases with concentration (Figure 5(a) and 5(d)), suggesting the adsorption of surfactant molecules at the interface. Furthermore, the C1s peaks can be deconvoluted into two distinct peaks with binding energies of approximately 286 eV and 284 eV. These two contributions represent carbon atoms bonded to heteroatoms (nitrogen or oxygen, 286 eV) denoted by C_{hetero}, and carbon atoms only bonded

to other carbons and hydrogen, denoted by C_{alkyl} (*16*). Even without performing peak-fitting calculations (for a detailed discussion of this procedure and its assumptions, see Lovelock et al. (*28*)), the intensity ratio of C_{alkyl}/C_{hetero} increases with concentration for both surfactants, confirming that adsorption at the interface is due to the surfactant. The changes in C1s peak intensity and C_{alkyl}/C_{hetero} ratio with concentration are more obvious for C_{14}TAB, which is probably due to the high surface activity of this longer chain surfactant. Consequently, the decreases in peak intensity for N1s and S2p signals (Figure 5(b), (c), (e), (f)) are also more pronounced for C_{14}TAB, with the latter decrease clearly attributable to the surfactant. These qualitative results that are obtained directly from the X-ray photoelectron spectra further support our above discussions.

Information Depth Effects

As mentioned previously, the various quantities calculated from the XPS data are spatial averages over an information depth that is determined by the emission angle. Here we define this angle to be between the detector and the surface normal, but we note that other conventions are sometimes used. The relationship between the emission angle θ and the information depth d is given by the expression $d \approx 3\lambda \cos\theta$ (*41*), where λ is the electron mean free path. Since λ varies with the element being considered, we take an average over C1s, N1s, and S2p to arrive at λ = 1.50 nm. By using a larger XPS emission angle, the information depth is reduced and hence we expect to observe a larger surface fraction of surfactant. However, using *too small an information depth is undesirable* because the resultant length scales would be less than the size of the surfactants and rule out the use of both atomic mass balance analysis *and* peak-fitting deconvolution. Therefore, we examined emission angles of 75°, 45°, and 30°, which correspond to information depths of 1.2 nm, 3.2 nm, and 3.9 nm, respectively. We note that the unit length of surfactant alkyl chain is 0.126 nm (*50*) so the fully extended surfactant chain length is between 0.63 nm (n=6) and 1.64 nm (n=14). The true chain dimensions will be somewhat smaller than the full extensions due to chain conformational flexibility and hence are expected to be within our information depths. In this regard, we emphasize once more that emission angles greater than 75° are not used since the information depth would be smaller than the thickness of surfactant monolayer at the interface.

In Figure 6, we use the difference in cation surface fractions $\Delta x^+ = C_nTA^+ - [EMIM]^+$ to summarize changes with concentration at various information depths. Both smaller and larger d show that with increasing surfactant concentration, the cation surface fraction difference Δx^+ is also increasing. This increase in Δx^+ is due to the fraction of C_nTA^+ increasing while the surface fraction of $[EMIM]^+$ is decreasing (see Figure 4). The value $\Delta x^+ = 0$ indicates the concentration corresponding to complete cation exchange. Clearly, this concentration shifts higher when larger d are used. On the other hand, at the smallest d studied, the larger surface fraction differences confirm that the surfactants are prone to stay close to the liquid-vapor interface.

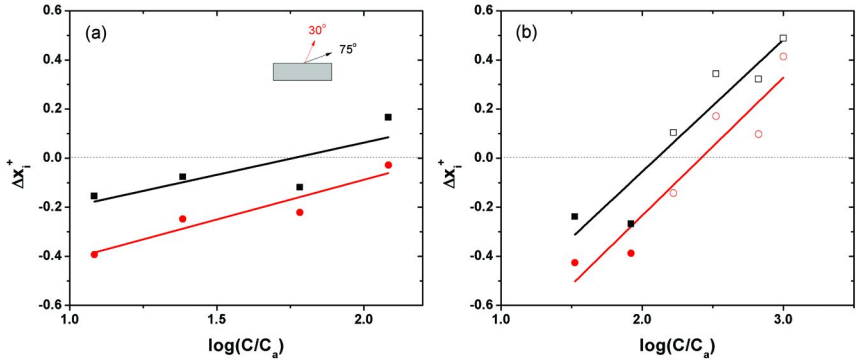

Figure 6. Surface fraction difference of cations $\Delta x^+ = C_nTA^+ - [EMIM]^+$, for (a) C_8TAB and (b) $C_{14}TAB$ in $[EMIM][EtSO_4]$. The emission angles of 75° (squares) and 30° (circles) correspond to information depths d of 1.2 nm and 3.9 nm, respectively. The open symbols represent samples that exhibit a semi-solid surface film.

Conclusions

In this work we examined the influence of charged surfactants in ionic liquids by XPS. Interfacial properties such as surface composition, charge, and enrichment were studied in terms of the surfactant alkyl chain length, concentration, and XPS information depth. Consistent with conventional tensiometry, our XPS results directly establish the surface activity of the surfactants and show that this quantity increases with alkyl chain length. We also find that an ion exchange process between like-charged surfactant and IL ions occurs at the interface, progressively increasing with surfactant concentration. Thus, surfactants can appreciably alter the interfacial properties of IL systems. By varying the XPS information depth *d*, we find that the effective surface activity increases inversely with *d*, confirming the tendency of the surfactant to remain close to the interface. Finally, we note that many opportunities remain to be explored with surfactant-IL mixtures, such as the role of counterions, nanoscale clustering in the bulk phase, and influences on layering near the interface. Although we have not done so here, careful angle-resolved XPS studies may show evidence of surfactant-induced surface layering that is distinct from the neat IL.

Acknowledgments

This work was financially supported by an NSF CAREER Award (DMR-0847558) to H.B., and by the NSF Materials Research Science and Engineering Center (DMR-0820506).

References

1. Welton, T. *Chem. Rev.* **1999**, *99*, 2071–2083.
2. Wasserscheid, P.; Keim, W. *Angew. Chem., Int. Ed.* **2000**, *39*, 3772–3789.
3. Yao, C.; Pitner, W. R.; Anderson, J. L. *Anal. Chem.* **2009**, *81*, 5054–5063.
4. Greaves, T. L.; Drummond, C. J. *Chem. Rev.* **2008**, *108*, 206–237.
5. Aliaga, C.; Santos, C. S.; Baldelli, S. *Phys. Chem. Chem. Phys.* **2007**, *9*, 3683–3700.
6. Fletcher, K. A.; Pandey, S. *Langmuir* **2004**, *20*, 33–36.
7. Zheng, L. Q.; Li, N.; Zhang, S. H.; Wu, J. P.; Li, X. W.; Yu, L. *J. Phys. Chem. B* **2008**, *112*, 12453–12460.
8. Li, N.; Zhang, S. H.; Zheng, L. Q.; Dong, B.; Li, X. W.; Yu, L. *Phys. Chem. Chem. Phys.* **2008**, *10*, 4375–4377.
9. Ogino, K.; Kakihara, T.; Abe, M. *Colloid Polym. Sci.* **1987**, *265*, 604–612.
10. Patrascu, C.; Gauffre, F.; Nallet, F.; Bordes, R.; Oberdisse, J.; de Lauth-Viguerie, N.; Mingotaud, C. *ChemPhysChem* **2006**, *7*, 99–101.
11. Smith, E. F.; Villar Garcia, I. J.; Briggs, D.; Licence, P. *Chem. Commun.* **2005**, 5633–5635.
12. Smith, E. F.; Rutten, F. J. M.; Villar-Garcia, I. J.; Briggs, D.; Licence, P. *Langmuir* **2006**, *22*, 9386–9392.
13. Gottfried, J. M.; Maier, F.; Rossa, J.; Gerhard, D.; Schulz, P. S.; Wasserscheid, P.; Steinruck, H. P. *Z. Phys. Chem.* **2006**, *220*, 1439–1453.
14. Lockett, V.; Sedev, R.; Bassell, C.; Ralston, J. *Phys. Chem. Chem. Phys.* **2008**, *10*, 1330–1335.
15. Kolbeck, C.; Cremer, T.; Lovelock, K. R. J.; Paape, N.; Schulz, P. S.; Wasserscheid, P.; Maier, F.; Steinruck, H. P. *J. Phys. Chem. B* **2009**, *113*, 8682–8688.
16. Lovelock, K. R. J.; Kolbeck, C.; Cremer, T.; Paape, N.; Schulz, P. S.; Wasserscheid, P.; Maier, F.; Steinruck, H. P. *J. Phys. Chem. B* **2009**, *113*, 2854–2864.
17. Maier, F.; Cremer, T.; Kolbeck, C.; Lovelock, K. R. J.; Paape, N.; Schulz, P. S.; Wasserscheidc, P.; Steinrueck, H.-P. *Phys. Chem. Chem. Phys.* **2010**, *12*, 1905–1915.
18. Maier, F.; Gottfried, J. M.; Rossa, J.; Gerhard, D.; Schulz, P. S.; Schwieger, W.; Wasserscheid, P.; Steinruck, H. P. *Angew. Chem., Int. Ed.* **2006**, *45*, 7778–7780.
19. Hofft, O.; Bahr, S.; Himmerlich, M.; Krischok, S.; Schaefer, J. A.; Kempter, V. *Langmuir* **2006**, *22*, 7120–7123.
20. Law, G.; Watson, P. R.; Carmichael, A. J.; Seddon, K. R.; Seddon, B. *Phys. Chem. Chem. Phys.* **2001**, *3*, 2879–2885.
21. Caporali, S.; Bardi, U.; Lavacchi, A. *J. Electron Spectrosc.* **2006**, *151*, 4–8.
22. Romero, C.; Baldelli, S. *J. Phys. Chem. B* **2006**, *110*, 6213–6223.
23. Jeon, Y.; Sung, J.; Bu, W.; Vaknin, D.; Ouchi, Y.; Kim, D. *J. Phys. Chem. C* **2008**, *112*, 19649–19654.
24. Solutskin, E.; Ocko, B. M.; Taman, L.; Kuzmenko, I.; Gog, T.; Deutsch, M. *J. Am. Chem. Soc.* **2005**, *127*, 7796–7804.
25. Law, G.; Watson, P. R. *Langmuir* **2001**, *17*, 6138–6141.

26. Carvalho, P. J.; Freire, M. G.; Marrucho, I. M.; Queimada, A. J.; Coutinho, J. A. P. *J. Chem. Eng. Data* **2008**, *53*, 1346–1350.
27. Ghatee, M. H.; Zolghadr, A. R. *Fluid Phase Equilibr.* **2008**, *263*, 168–175.
28. Lovelock, K. R. J.; Villar-Garcia, I. J.; Maier, F.; Steinruck, H. P.; Licence, P. *Chem. Rev.* **2010**, *110*, 5158–5190.
29. Niedermaier, I.; Kolbeck, C.; Taccardi, N.; Schulz, P. S.; Li, J.; Drewello, T.; Wasserscheid, P.; Steinruck, H. P.; Maier, F. *ChemPhysChem* **2012**, *13*, 1725–1735.
30. Hurisso, B. B.; Lovelock, K. R. J.; Licence, P. *Phys. Chem. Chem. Phys.* **2011**, *13*, 17737–17748.
31. Silvester, D. S.; Broder, T. L.; Aldous, L.; Hardacre, C.; Crossley, A.; Compton, R. G. *Analyst* **2007**, *132*, 196–198.
32. Liu, Q. B.; Janssen, M. H. A.; van Rantwijk, F.; Sheldon, R. A. *Green Chem.* **2005**, *7*, 39–42.
33. Wasserscheid, P.; Keim, W. *Angew. Chem., Int. Ed.* **2000**, *39*, 3772–3789.
34. Jacquemin, J.; Husson, P.; Majer, V.; Padua, A. A. H.; Gomes, M. F. C. *Green Chem.* **2008**, *10*, 944–950.
35. Domanska, U. *Pure Appl Chem* **2005**, *77*, 543–557.
36. Swatloski, R. P.; Spear, S. K.; Holbrey, J. D.; Rogers, R. D. *J. Am. Chem. Soc.* **2002**, *124*, 4974–4975.
37. Blesic, M.; Lopes, J. N. C.; Gomes, M. F. C.; Rebelo, L. P. N. *Phys. Chem. Chem. Phys.* **2010**, *12*, 9685–9692.
38. Roscioli, J. R.; Nesbitt, D. J. *J. Phys. Chem. Lett.* **2010**, *1*, 674–678.
39. Jones, R. A. L. *Soft Condensed Matter*; Oxford University Press: Oxford, 2002.
40. Fernandez, A.; Torrecilla, J. S.; Garcia, J.; Rodriguez, F. *J. Chem. Eng. Data* **2007**, *52*, 1979–1983.
41. Chen, L. G.; Lerum, R. V.; Aranda-Espinoza, H.; Bermudez, H. *J. Phys. Chem. B* **2010**, *114*, 11502–11508.
42. Sarkar, S.; Pramanik, R.; Ghatak, C.; Setua, P.; Sarkar, N. *J. Phys. Chem. B* **2010**, *114*, 2779–2789.
43. Chen, L. G.; Bermudez, H. *Langmuir* **2012**, *28*, 1157–1162.
44. Marsh, K. N.; Boxall, J. A.; Lichtenthaler, R. *Fluid Phase Equilibr.* **2004**, *219*, 93–98.
45. Strutt, J. W. *Philos. Mag.* **1899**, 321–337.
46. Gomez-Diaz, D.; Navaza, J. M.; Sanjurjo, B. *J. Chem. Eng. Data* **2007**, *52*, 889–891.
47. Mukerjee P, M. K. *Critical Micellar Concentration of Aqueous Surfactant Systems*; National Bureau of Standards: Washington, DC, 1971.
48. Hougen, O. A. *Chemical Process Principles*; Wiley: New York, 1954.
49. Felder, R. M.; Rousseau, R. W. *Elementary Principles of Chemical Processes*; John Wiley: New York, 1999.
50. Israelachvili, J. N. *Intermolecular and Surface forces*; Academic Press: San Diego, 1992.
51. Rebelo, L. P. N.; Lopes, J. N. C.; Esperanca, J. M. S. S.; Guedes, H. J. R.; Lachwa, J.; Najdanovic-Visak, V.; Visak, Z. P. *Accounts Chem. Res.* **2007**, *40*, 1114–1121.

52. Mosquera, V.; del Rio, J. M.; Attwood, D.; Garcia, M.; Jones, M. N.; Prieto, G.; Suarez, M. J.; Sarmiento, F. *J. Colloid. Interf. Sci.* **1998**, *206*, 66–76.
53. Lynden-Bell, R. M. *Phys. Chem. Chem. Phys.* **2010**, *12*, 1733–1740.
54. Ueno, K.; Tokuda, H.; Watanabe, M. *Phys. Chem. Chem. Phys.* **2010**, *12*, 15133–15134.
55. Ueno, K.; Inaba, A.; Kondoh, M.; Watanabe, M. *Langmuir* **2008**, *24*, 5253–5259.
56. Angell, C. A.; Byrne, N.; Belieres, J. P. *Acc. Chem. Res.* **2007**, *40*, 1228–1236.
57. Wang, Y. T.; Voth, G. A. *J. Am. Chem. Soc.* **2005**, *127*, 12192–12193.
58. Wang, Y.; Jiang, W.; Yan, T.; Voth, G. A. *Acc. Chem. Res.* **2007**, *40*, 1193–1199.
59. Lynden-Bell, R. M.; Del Popolo, M. G.; Youngs, T. G. A.; Kohanoff, J.; Hanke, C. G.; Harper, J. B.; Pinilla, C. C. *Acc. Chem. Res.* **2007**, *40*, 1138–1145.
60. Triolo, A.; Russina, O.; Bleif, H. J.; Di Cola, E. *J. Phys. Chem. B* **2007**, *111*, 4641–4644.
61. Bhargava, B. L.; Balasubramanian, S. *J. Am. Chem. Soc.* **2006**, *128*, 10073–10078.